energies

MDPI

Article

Dynamic Investigation of a Coupled Parabolic Trough Collector–Phase Change Material Tank for Solar Cooling Process in Arid Climates

Abdelhamid Ajbar [1], Bilal Lamrani [2,*] and Emad Ali [1,*]

[1] Chemical Engineering Department, King Saud University, Riyadh 11451, Saudi Arabia; aajbar@ksu.edu.sa
[2] Laboratoire MANAPSE, Faculté des Sciences, Université Mohammed V de Rabat, P.O. Box 1014, Rabat 10000, Morocco
* Correspondence: b.lamrani@um5r.ac.ma (B.L.); amkamal@ksu.edu.sa (E.A.)

Abstract: The use of solar energy for cooling processes is advantageous for reducing the energy consumption of conventional air-conditioning systems and protecting the environment. In the present work, a solar-powered cooling system with parabolic trough collectors (PTC) and a phase change material (PCM) tank is numerically investigated in the arid climates of Saudi Arabia. The system contains a 160-kW double-effect absorption chiller powered by solar-heated pressurized water as a heat transfer fluid (HTF) and a shell and tube PCM as a thermal battery. The novelty of this paper is to investigate the feasibility and the potential of using a PTC solar field coupled to a PCM tank for cooling purposes in arid climates. The numerical method is adopted in this work, and a dynamic model is developed based on the lumped approach; it is validated using data from the literature. The functioning of the coupled system is investigated in both sunshine hours (charging period) and off-sunshine hours (discharging period). The PTC area in this work varies from 200 m^2 to 260 m^2 and the cooling capacity of the chiller ranges from 120 kW to 200 kW. Obtained results showed that the 160-kW chiller is fully driven by the 240 m^2-solar PTC during the charging period and about 23% of solar thermal energy is stored in the PCM tank. It was demonstrated that increasing the PTC area from 220 m^2 to 260 m^2 leads to a reduction in the PCM charging time by up to 45%. In addition, it was found that an increase in the cooling loads from 120 kW to 200 kW induces a decrease in the stored thermal energy in the PCM tank from 450 kWh to 45 kWh. During the discharging period, the PCM tank can continue the cooling process with a stable delivered cooling power of 160 kW and an HTF temperature between 118 °C and 150 °C. The PCM tank used in the studied absorption chiller leads to a reduction of up to 30% in cooling energy consumption during off-sunshine hours.

Keywords: parabolic trough collector; double-effect absorption chiller; phase change material; solar-powered cooling

Citation: Ajbar, A.; Lamrani, B.; Ali, E. Dynamic Investigation of a Coupled Parabolic Trough Collector–Phase Change Material Tank for Solar Cooling Process in Arid Climates. *Energies* **2023**, *16*, 4235. https://doi.org/10.3390/en16104235

Academic Editor: Philippe Leclère

Received: 19 April 2023
Revised: 11 May 2023
Accepted: 15 May 2023
Published: 22 May 2023

1. Introduction

In hot regions, heating, ventilating and air-conditioning (HVAC) systems are known to consume the largest part of electricity [1,2]. In Saudi Arabia, for example, it was reported that as much as 40% of the total electricity is used to cool commercial buildings [3]. The International Energy Agency (IEA) also predicted that by 2050 about two-thirds of the world's buildings will be equipped with air-conditioning systems [4]. Presently, there is tremendous research on the utilization of renewable energy (especially solar energy) for cooling. This interest stems from the desire to reduce dependence on fossil fuels and to cut down on energy bills.

A solar cooling system consists of three main elements: (1) a solar collector, (2) a refrigeration system and (3) a heat sink. The main solar cooling and air-conditioning systems are mainly of three types: solar absorption, solar adsorption and solar desiccant systems. In absorption cycles, the cooling process depends on the evaporative cooling of a

refrigerant. Desiccant cooling systems depend on cycling dehumidification–humidification processes while the solar mechanical cycles combine conventional cooling systems with solar-powered mechanics.

Solar cooling has the potential benefit of providing cooling systems to countries that are unable to cope with the high costs of conventional cooling systems. However, as mentioned by Alahmer et al. [5], solar cooling and air-conditioning systems are yet to gain a competitive edge over traditional electric-driven vapor compression cycle systems. This is due to higher capital costs, lower performance and intermittent availability of solar energy. Despite these limitations, research should continue towards overcoming these challenges through novel and smart configurations.

A large number of studies are available in the literature on solar cooling systems. Aljuhani and Abdel Dayem [6], for instance, carried out the design of a solar absorption cooling system combined with a chilled water system for a hypothetical pilgrimage tent in Saudi Arabia. Al-Ugla et al. [7] discussed the performance of three types of energy storage used in solar absorption systems. Their analysis found that the largest collector area and the smallest mass are required for the cold storage system. By comparison, the hot storage system had the highest mass required and the highest coefficient of performance when used at night. Rahman et al. [8] carried out simulations of an absorption-type solar air-conditioning system for the city of Lahore, Pakistan. Habib et al. [9] used TRNSYS software to simulate an integrated absorption system. Rahman et al. [10] designed a solar energy absorption system for the United Arab Emirates weather. Ramadas et al. [11] studied the use of a solar absorption chiller for student residential buildings in Australia. Lahoud et al. [12] examined the use of a single-effect absorption chiller. Moreover, the authors carried out a thermo-economic feasibility analysis for a 700-kW sports stadium. The use of phase change materials (PCMs) as a storage medium is advantageous for concentrated solar power technologies [13]. Mohamed Ali et al. [14,15] have shown the potential of using the PCM tanks to reduce energy consumption and to overcome the problem of a mismatch between energy supply and energy demand. Recently, a solar cooling system using sensible thermal storage and evacuated tube collectors was proposed by Yadav et al. [16]. The system is designed to drive a combined cooling and power system. Ghaith and Dag [17] have investigated the feasibility of using ice as a sensible storage medium for space cooling applications. They found that the use of this thermal storage system contributed to significant savings in annual electricity consumption.

We can conclude from this short review that most of the published works are focused only on the use of the following: (1) single-effect solar absorption chillers, (2) ordinary flat plate solar collectors or evacuated tube collectors and (3) conventional sensible storage in water or oil tanks. The main contribution of this work is to numerically investigate a novel double-effect absorption chiller system powered by a solar concentrator (parabolic trough collectors) and a latent PCM storage tank. This proposed coupled solar-powered cooling system with PCM thermal storage could be advantageous to reduce the energy consumption of conventional air-conditioning systems during both daytime and nighttime operations. Parabolic trough collectors (PTCs) are used mainly to capture solar energy and to produce hot pressurized water for driving a double solar absorption chiller system for air-conditioning. Since the heat transfer fluid is pressurized water, the system can also be used during cooled periods to produce hot water and satisfy the heating requirements.

2. Solar-Powered Cooling System Description

The proposed solar-powered system for cooling applications is illustrated in Figure 1. This solar system is composed of PTCs, a latent heat storage system in a PCM tank and a double-effect solar absorption chiller system for air-conditioning. The main advantage of this proposed system is its ability to provide the needed thermal energy for operating the solar absorption chiller during sunshine and off-sunshine hours. In addition, this proposed system can also be used during the cold periods of the year (no cooling needs) for the hot water production process, as the used heat transfer fluid (HTF) is pressurized water. In

this paper, the performance of this solar system is investigated during the hot periods of the year in Riyadh (Saudi Arabia), and it is used mainly for driving a double-effect solar absorption chiller. The functioning mechanism of the investigated solar system can be described as the following:

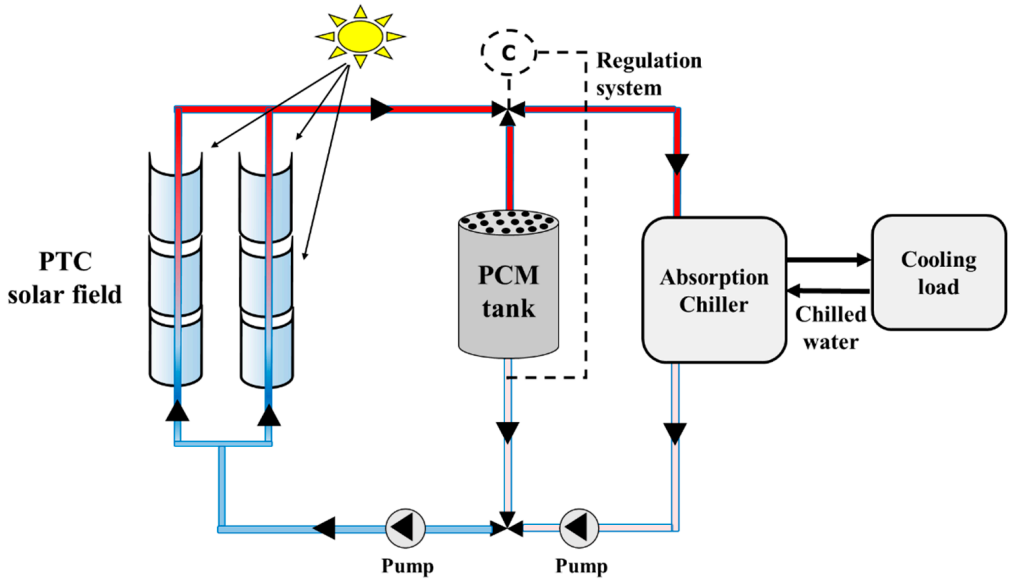

Figure 1. Schema of the proposed solar power system during the charging period.

2.1. Charging and Cooling Period

During this period (sunshine hours), HTF (pressurized water) passes through the absorber tube of the PTC where it receives direct solar irradiations. The heated HTF at the outlet of the PTC is then directed simultaneously to both the PCM tank for storing the thermal energy produced in excess and to the generator of the chiller for the cooling process. The PCM tank is composed of concentric cylinders where the HTF circulates in the inner tubes and the PCM fills in the space between the tubes and the shell. The heat is transferred from the hot HTF to the PCM, and the thermal energy is stored in both sensible and latent forms (phase change process from solid to liquid state). More details about the functioning of the used PCM tank are given in Section 3.2. In the absorption chiller side, the hot HTF provides the necessary heat for driving the chiller generator and to maintain the stable operation of the solar air-conditioning system. The considered commercial water-lithium bromide (H_2O-LiBr) absorption chiller type has a nominal cooling capacity of 160 kW and an average coefficient of performance (COP) of 1.3 [12]. It is interesting to note this double-effect absorption chiller is chosen due to its high COP compared to the single-effect absorption chiller and its ability to provide high cooling capacities [3,18]. The characteristics of the considered water-lithium bromide double-effect absorption chiller are summarized in Table 1. At the outlet of both the chiller generator and the PCM storage tank, the HTF is recovered and then transferred to the PTC solar loop for receiving solar heat, increasing its temperature. It can be noted that this charging and cooling period is activated when the thermal energy produced by the PTC solar collector is higher than 120 kW and the HTF temperature is between 110 °C and 170 °C. This operation condition will allow the solar cooling system to produce 160 kW of cooling power and to store the excess thermal energy produced in the PCM tank for later use.

Table 1. Properties of the used commercial absorption chiller BROAD model [19].

Characteristic	Value
Cooling capacity	160 kW
COP	1.33
Generator operation temperature (T_g)	110–170 °C
Outlet temperature at the generator	T_g − 10 °C
Generator flow rate	2.87 kg/s
Inlet temperature at the evaporator	12 °C
Outlet temperature at the evaporator	7 °C
Evaporator flow rate	7.7 kg/s
Inlet temperature at the condenser	30 °C
Outlet temperature at the condenser	37 °C

2.2. Discharging and Cooling

During this period (off/low-sunshine hours), the solar field is defocused and the circulation of the HTF in the PTC is stopped. The schematic of the operated system during this period is illustrated in Figure 2. The PCM tank is used as the heat source to extend the functioning of the absorption chiller during this period and therefore continue the cooling process using the stored thermal energy. It is important to note that the stored thermal energy will be used to cover only a part of the required thermal energy for the cooling process and will thus reduce the energy consumption of the absorption chiller. During this process, both sensible and latent heat stored in the tank are released and the PCM changes its phase from liquid state to solid state. This thermal energy is recovered by the HTF and then passed through the chiller generator for chilled water production. If the storage tank is fully discharged (complete solidification of the PCM) and the produced HTF temperature is not sufficient to drive the chiller machine, the absorption machine auxiliary heater is turned on and the required additional heat is produced for the cooling process. Through this operation strategy, the absorption chiller energy consumption will be minimal, and its energy efficiency will be improved.

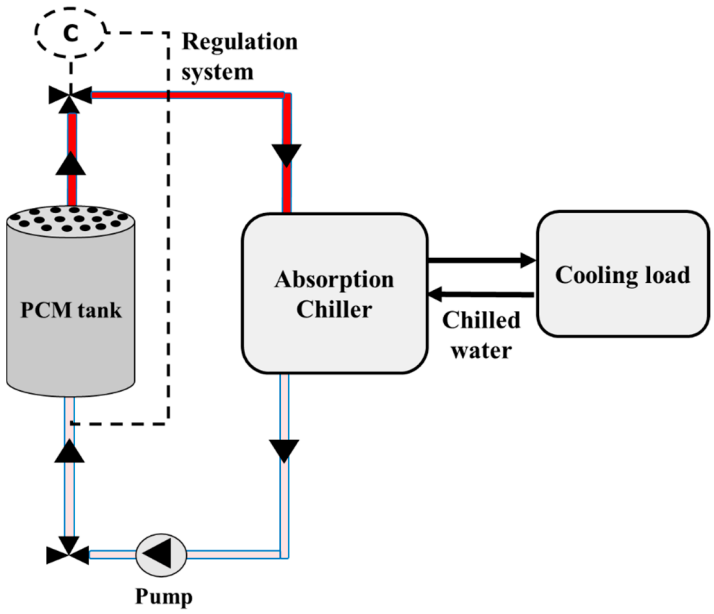

Figure 2. Schema of the proposed solar power system during the discharging period.

3. Model Development and Verification

3.1. PTC Model

This concentrated type of solar collector (PTC) is able to produce HTF temperatures in the range of 60–300 °C with high thermal efficiency compared to traditional flat plate

and evacuated tube solar collectors [20–23]. This type of solar collector is chosen in this work due to its suitable temperature range for supplying the necessary thermal energy to drive the chiller generator and to ensure a complete charging process of the PCM tank with high phase transition temperatures (higher than 100 °C). In fact, using traditional flat plate collectors leads to the production of low HTF temperatures, i.e., between 30 and 80 °C, which is not suitable for double-effect solar absorption chillers (See Table 1). The used PTC in the present study is able to produce the needed HTF temperature range (110 °C to 170 °C), and it contains a reflected mirror, a receiver tube and a sun-tracking unit. The characteristics of the commercial PTC (Eurotrough ET-150 [24]) used in this work are given in Table 2. During the functioning of this solar collector, the received direct normal irradiation is first reflected and then absorbed by the receiver tube. The absorbed heat is then transferred by conduction and by convection to the HTF (pressurized water) and this leads to an increase in its temperature. A cross-section of the used PTC is illustrated in Figure 3.

Table 2. Used parameters of one PTC unit in the proposed solar system.

Parameter	Value
Area [m^2]	200, 220, 240, 260
Absorber diameter [m]	0.034
Absorber thickness [m]	0.002
Glass cover diameter [m]	0.056
Glass cover thickness [m]	0.0025
Absorber absorptance	0.9
Absorber emittance	0.14
Glass cover transmittance	0.95
Glass cover emittance	0.86
Angle modifier $K(\theta)$	1

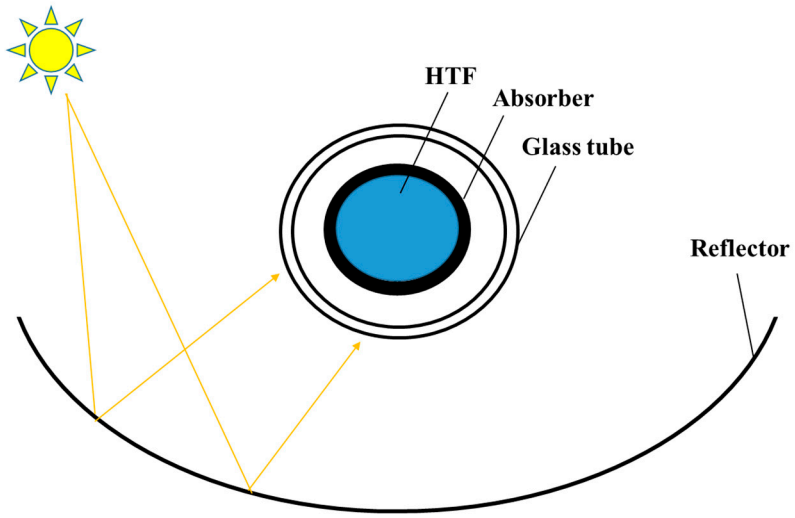

Figure 3. PTC cross-section.

To predict the functioning of the considered solar PTC, the beam irradiation (G_b) is used as the received solar irradiation of the PTC aperture area (A_c), and the useful solar irradiance by the PTC is computed as follows:

$$Q_{solar} = A_c G_b \quad (1)$$

The useful thermal power of the pressurized water (working fluid) between the inlet and the outlet of the PTC collector can be determined using Equation (2):

$$Q_u = \dot{m}_{HTF} C_p (T_{out} - T_{inlet}) \quad (2)$$

where $\dot{m}_{HTF}$ is the HTF mass flow rate, and C_p is the HTF heat capacity. T_{out} and T_{inlet} are the HTF outlet and inlet temperatures, respectively.

The thermal efficiency of the PTC collector is defined as the ratio between the useful thermal power of the HTF to the received solar power, as shown in the following equation [21]:

$$\eta_{th} = \frac{Q_u}{Q_{solar}} \quad (3)$$

In this investigation, the thermal efficiency equation for a commercial PTC (Eurotrough ET-150) is used. This equation establishes a relationship between the thermal efficiency, the ambient temperature, the used solar beam irradiance and the temperature of the HTF at the PTC inlet. This equation is given as the following [24,25]:

$$\eta_{th} = 0.74K(\theta) - 0.000045(T_{inlet} - T_{amb}) - 0.039\left(\frac{T_{inlet} - T_{amb}}{G_b}\right) - 0.003G_b\left(\frac{T_{inlet} - T_{amb}}{G_b}\right)^2 \quad (4)$$

By solving all previous equations (Equations (1)–(4)), the PTC thermal performances are simulated by calculating thermal efficiency and the HTF temperature at the outlet. To verify the accuracy of this thermal model, obtained numerical results were compared with experimental from references [26,27]. Figure 4 shows that the model can predict the real behavior of the PTC with a maximal relative error of 5%.

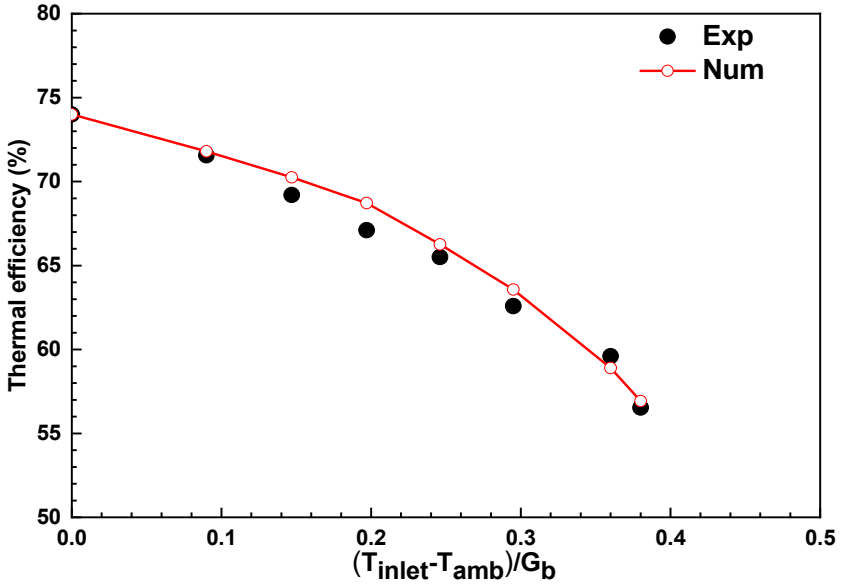

Figure 4. Variation of numerical and experimental PTC thermal efficiency from [26,27].

3.2. PCM Tank Model

Using a latent heat storage system for solar applications is known as an efficient way to minimize the mismatch between energy supply and energy demand and to extend the operation of these solar-powered systems during the off/low-sunshine hours. In this work, the PCM tank is used for the solar cooling application, and it is coupled to the solar field during the charging process (daytime period) and to the generator absorption chiller for the discharging process (off/low-sunshine period). The studied PCM tank is a shell-and-tube heat exchanger where the HTF circulates in the inner tubes, and the PCM fills in the empty space between tubes (Figure 5). During the charging process, the HTF

coming from the solar field with a high temperature enters the PCM tank and the flow is divided into the tubes. Heat is transferred from the HTF to the PCM, and this leads to an increase in its temperature and stores the heat in the sensible form. If the PCM temperature reaches the phase transition temperature, the fusion of the PCM starts and the heat is stored in the latent form at nearly constant temperature. At the end of the charging process, the PCM temperature will be higher than its melting point, and its physical state will be liquid. During the discharging process, the HTF coming from the solar field is stopped, and the PCM tank is used for driving the solar chiller generator. In this period, the HTF circulates between the PCM tank and the chiller generator, and the heat is transferred from the PCM to the HTF (solidification process of the PCM). This recovered thermal energy will be used to extend the functioning of the solar chiller and to cover a part of its energy consumption during off/low-sunshine hours. The choice of a suitable PCM for this application is an important design step, and its transition temperature is one of the main factors to be considered. In fact, the PCM melting point must be chosen based on the required temperature for driving the chiller generator. According to the technical operation parameters of the commercial double-effect absorption chiller, the required temperature of the generator must be between 110 and 170 °C. Based on these operation temperatures, A118 from the PlusICE® company (Yaxley, Peterborough, UK) was chosen as a commercial PCM with a transition temperature between 117 °C and 119 °C. In addition to this criterion, the chosen PCM must also have a high latent heat of fusion [21,28] and a high thermal conductivity [29]. The design of the tank and thermophysical properties of the chosen commercial PCM (A118) are summarized in Table 3.

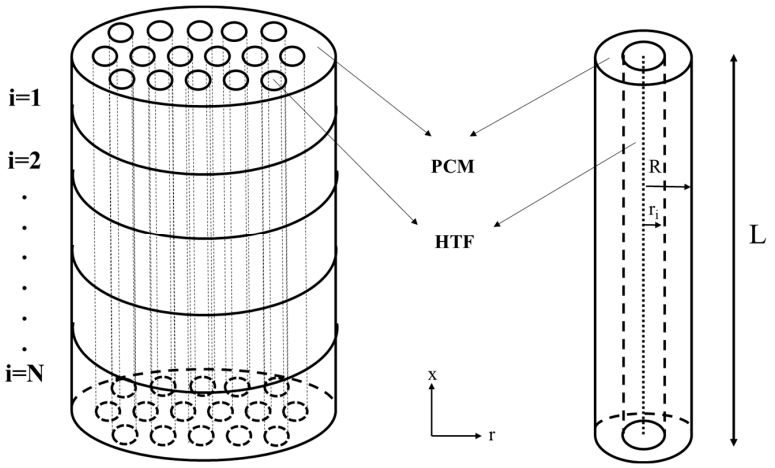

Figure 5. The studied PCM storage tank for the solar cooling system.

Table 3. Properties of the considered PCM in the proposed solar system [30].

Properties	Value
Thermal conductivity (W/m·K)	0.22
Density (kg/m^3)	900
Transition temperature (°C)	117–119
Specific heat capacity (J/kg·K)	2200
Latent heat capacity (kJ/kg)	195
PCM tank volume (m^3)	2.446
PCM tank length (m)	3.42
Number of tubes in the PCM tank (-)	400
Tube diameter in the PCM tank (m)	0.036

To model the dynamic behavior of the PCM tank, the lumped-capacitance approach is adopted. The latter has several advantages and is characterized by its fast calculation time [31,32] where only ordinary differential equations (ODEs) are solved instead of solving

complex differential equations (PDEs) [33,34]. The ODEs are constructed by applying energy balances for each component of the PCM tank, i.e., the PCM domain and the HTF domain. To determine the space-time variation of the temperature inside the PCM tank, the latter is divided into several horizontal control volumes (See Figure 5) where the energy balance is applied in each control volume. It is important to note that during the application of the lumped approach, the temperature in each control volume is assumed to be uniform and the HTF flow is considered to be unidirectional. The energy balances can be expressed as the following:

- Control volume 1 (HTF):

$$\left(mC_p\right)_{f,1}\frac{\partial T_{f,1}}{\partial t} = h_f A\left(T_{st,1} - T_{f,1}\right) + \dot{m}_f C_{p,f}\left(T_{f,inlet,1} - T_{f,out,1}\right) \quad (5)$$

- Control volume 1 (PCM):

$$\left(mC_p\right)_{st,1}\frac{\partial T_{st,1}}{\partial t} = h_f A\left(T_{f,1} - T_{st,1}\right) \quad (6)$$

- Control volume 2 (HTF):

$$\left(mC_p\right)_{f,2}\frac{\partial T_{f,2}}{\partial t} = h_f A\left(T_{st,2} - T_{f,2}\right) + \dot{m}_f C_{p,f}\left(T_{f,inlet,2} - T_{f,out,2}\right) \quad (7)$$

- Control volume 2 (PCM):

$$\left(mC_p\right)_{st,2}\frac{\partial T_{st,2}}{\partial t} = h_f A\left(T_{f,2} - T_{st,2}\right) \quad (8)$$

- Control volume N (HTF):

$$\left(mC_p\right)_{f,N}\frac{\partial T_{f,N}}{\partial t} = h_f A\left(T_{st,N} - T_{f,N}\right) + \dot{m}_f C_{p,f}\left(T_{f,inlet,N} - T_{f,out,N}\right) \quad (9)$$

- Control volume N (PCM):

$$\left(mC_p\right)_{st,N}\frac{\partial T_{st,N}}{\partial t} = h_f A\left(T_{f,N} - T_{st,N}\right) \quad (10)$$

where T_f and T_{st} are the HTF temperature and the PCM temperature of each control volume, respectively. A is the exchange heat transfer area, and $\dot{m}_{HTF}$ is the HTF mass flow rate in the PCM tank. It is interesting to note that the HTF temperature at the outlet of a control volume (i) is considered equal to the input temperature of the control volume ($i + 1$). The used convective heat transfer coefficient (h_f) is determined using the following equation [15,29]:

$$h_f = \frac{k_f}{D_h}\begin{cases} 4.36 & R_e \leq 2300 \\ \frac{\left(\frac{f}{8}\right)(R_e - 1000)P_r}{1 + 12.7\left(\frac{f}{8}\right)^{0.5}\left((P_r)^{\frac{2}{3}} - 1\right)} & R_e > 2300 \end{cases} \quad (11)$$

To simulate the phase change phenomena in the PCM during the functioning of the solar-powered system, the effective heat capacity method is used. The approach used for

modeling is based on the use of an equivalent PCM heat capacity where its value depends on the PCM temperature. The expression of the PCM heat capacity is given by [35,36]:

$$C_{p,pcm}(T) = C_{base}(T) + C_{excess}(T) \tag{12}$$

where:

$$C_{base}(T) = C_{p,s}(T) + C_{p,l}(T) \tag{13}$$

$$C_{excess}(T) = L_s \frac{\partial f(T)}{\partial T} \tag{14}$$

In the previous expression, the PCM heat of fusion is denoted by L_s, and the PCM average liquid fraction is denoted by $f(T)$. When the PCM temperature is lower than the melting one, the $f(T)$ is equal to zero and the C_{base} is equal to the solid PCM heat capacity ($C_{p,s}$). However, if the PCM temperature is higher than the melting point, the $f(T)$ is equal to one and the C_{base} is equal to the liquid PCM heat capacity ($C_{p,l}$). During the phase transition period, i.e., $0 < f(T) < 1$, the PCM liquid fraction is given by:

$$f(T) = \frac{1}{\pi}\left[arctan\left[\frac{2\gamma(T - T_m)}{\Delta T}\right] + \frac{\pi}{2}\right] \tag{15}$$

This expression of the PCM liquid fraction is integrated into Equation (12) and the final expression of the PCM heat capacity can be expressed as:

$$C_{p,pcm}(T) = C_{base}(T) + L_s \frac{\frac{2\gamma}{\Delta T}}{\pi\left[\left((T - T_m)\left(\frac{2\gamma}{\Delta T}\right)\right)^2 + 1\right]} \tag{16}$$

All the previous coupled equations were implemented in EES code (Engineering Equation Solver) [37]. This tool was chosen mainly due to its ability to solve several coupled ordinary differential equations, and it offers users routines to calculate the thermodynamic properties of various heat transfer fluids.

To ensure the validity of both the PCM modeling approach and the PCM tank dynamic global model, obtained results were compared with experimental results from the literature [35,36,38]. Medved et al. [35] have experimentally measured the variation of the PCM heat capacity with the temperature. The same design and operation conditions were used as input parameters in the developed EES code, and the obtained results were compared with measured data. Figure 6a shows the variation of the PCM heat capacity with the temperature using the developed model and measured data from the reference [35]. This result indicates that the proposed approach can estimate with good accuracy the PCM heat capacity variation in both the sensible heat transfer domain (constant low values of *Cp*) and the latent heat transfer domain (a jump of *Cp* with *T*). This validated PCM heat capacity function is used in the PCM tank model, and the simulation results were compared with real-scale shell-and-tube PCM tank measurements [38]. The present PCM tank has the same used design in the experimental work of [33] where it is used to provide hot water for a district heating substation in France. More details about this study could be found in our previously published works [34,39]. By using the same previous validation methodology, obtained results from the proposed dynamic model were compared with the experimental measurements, and the obtained results are given in Figure 6b. By analyzing this result, it can be seen that the PCM tank model predicts with acceptable accuracy the real dynamic thermal behavior of the storage system. The maximum relative error is equal to 5%. In fact, the produced water temperature from the PCM tank model follows the measured one, where it decreases until reaching the phase transition period. During this period, both the simulated and the measured outlet water temperatures become stable due to the high amount of produced latent thermal energy from the PCM. At the end of the phase change process, the water temperature drops, and only sensible thermal energy is released.

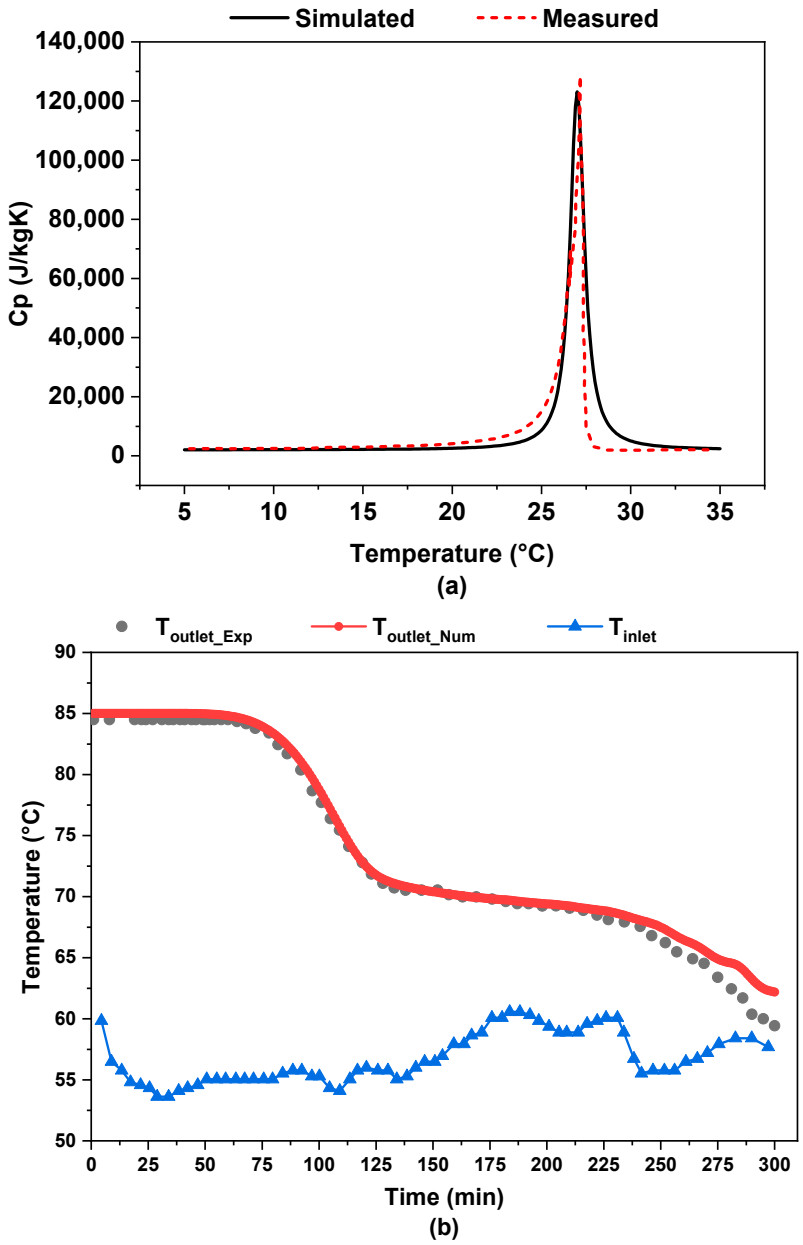

Figure 6. (**a**) PCM heat capacity method validation: numerical results vs. measured data [36], (**b**) PCM tank numerical results vs. experimental results from [38].

Finally, and based on the previous validation studies, it can be concluded that the proposed dynamic models for both the PTC solar system and the PCM tank are validated and can be used to successfully predict the dynamic behavior of these systems. These models will be used in the following section to produce and store renewable thermal energy for the solar cooling process in Riyadh (Saudi Arabia). This renewable thermal energy will be mainly used in the generator of a double-effect absorption chiller with a cooling capacity of 160 kW, and a generator operation temperature between 110 °C and 170 °C [19].

4. Results and Discussion

In this section, the dynamic thermal behavior of the studied solar-powered cooling system is investigated in the meteorological conditions of Riyadh. The solar thermal system is designed to deliver 120 kW of thermal power to drive the chiller generator and produce 160 kW of cooling power (COP = 1.33) during a representative day of the summer season (21 June). The excess produced solar thermal energy from the PTC solar field will be stored

in the PCM tank. This stored thermal energy will be used to extend the operation of the absorption chiller during low- or off-sunshine hours, thus reducing its energy consumption.

4.1. Weather Data and Operation Conditions

As mentioned previously, the proposed solar-powered system is investigated using the weather data of Riyadh. The monthly variation of solar radiation and ambient temperature is given in Figure 7a. These data show that Riyadh is characterized by a hot climate from April to September, which will induce a high cooling energy demand. The maximal monthly air temperature during this hot period is reached between June and August, and it is up to 38 °C. The maximal monthly solar radiation is reached during the same period of the year, particularly in June, with a value of 236 kWh/m^2. These data confirm two points. The first is that the energy consumption for the cooling process of buildings and industrial sectors will be high during this period. The second is that using solar cooling systems in such weather conditions will be advantageous and could significantly reduce the high energy consumption, protecting the environment. As June is the hottest month of the year in Riyadh, a representative day of summer (21 June) from this month will be used as an input parameter in the developed dynamic model. The hourly variation of the beam solar irradiance and the ambient temperature are plotted in Figure 7b. It can be observed that the maximal ambient temperature during this day can reach 43 °C at 3 p.m., and the maximal direct solar irradiance is up to 905 W/m^2. These data are used as input parameters to simulate the real functioning of the PTC. This high amount of received solar irradiance could be used successfully to power the chiller generator by providing the necessary thermal energy for the solar cooling process.

By using these previous meteorological data of the representative summer day, the variation of the produced solar thermal power from the PTC field is presented in Figure 8. It can be seen that the solar PTC field is able to provide the necessary thermal energy for driving the chiller generator. In fact, the produced solar thermal energy follows the solar irradiance behavior and reaches a value higher than 120 kW (necessary thermal energy for the cooling process) from 9 a.m. to 5 p.m. During this period, the PCM tank can be used as a thermal battery for the storage of excess produced solar thermal energy and to maintain a stable operation of the solar cooling process. During the early morning or in the late afternoon, this stored thermal energy in the PCM tank will be used when the produced solar thermal power is insufficient (lower than 120 kW) to meet the cooling power demand. Figure 8 shows also the hourly variation of the PTC solar field thermal efficiency. During sunshine hours, the PTC thermal efficiency varies between 73% and 74% as the received solar energy is lost due to the reflection coefficient of the PTC mirror and the convection heat losses between the PTC receiver and the exterior air.

4.2. Charging and Cooling Period

The charging and cooling period refers to the period of the day when the produced solar thermal power from the PTC field is higher than the required power to drive the chiller generator. This period is fixed in the representative summer day in Riyadh from 9 a.m. to 4 p.m., i.e., 420 min. During this period, both the solar irradiance and the ambient temperature in the city reach their maximal values, and therefore the cooling demand will be high. The variation of the instantaneous thermal power at the PTC solar field, at the PCM tank and at the cooling generator are given in Figure 9a. It is interesting to note that the used PTC area is equal to 240 m^2. The obtained results show that the maximal value of produced solar thermal power can reach 160 kW during this period. By using the PCM tank, this excess of produced solar thermal power is stored, and therefore the chiller generator operates in a stable condition with a fixed thermal power of 120 kW. This proposed design operation is advantageous for solar-powered systems as it maintains the stable operation of the solar cooling system under variable solar radiation and without using any additional regulation or auxiliary system. The cumulated thermal energy in the investigated solar system is shown in Figure 9b. It can be shown that most of the produced solar thermal

energy from the PTC field is used to drive the chiller generator for the cooling process and the rest of the produced thermal energy is stored in the PCM for later use. At the end of the charging and cooling operation, about 77% of the produced solar thermal energy is used for the cooling process and 23% is stored in the PCM tank. The diagram of the energy flow during the charging and cooling period is illustrated in Figure 10. It can be seen clearly that not all the available solar energy is used in the solar-powered system, but only 73% of it is used by the PTC for thermal energy production. These energy losses are due to the temperature difference between the PTC absorber and the environment and are due to the PTC optical losses. As the nominal COP of the used commercial double-effect absorption chiller is 1.33, the used thermal energy at the generator is converted into cooling thermal energy and increased from 836 kWh to 1114 kWh. The rest of the produced thermal energy of about 250 kWh is stored in the PCM tank.

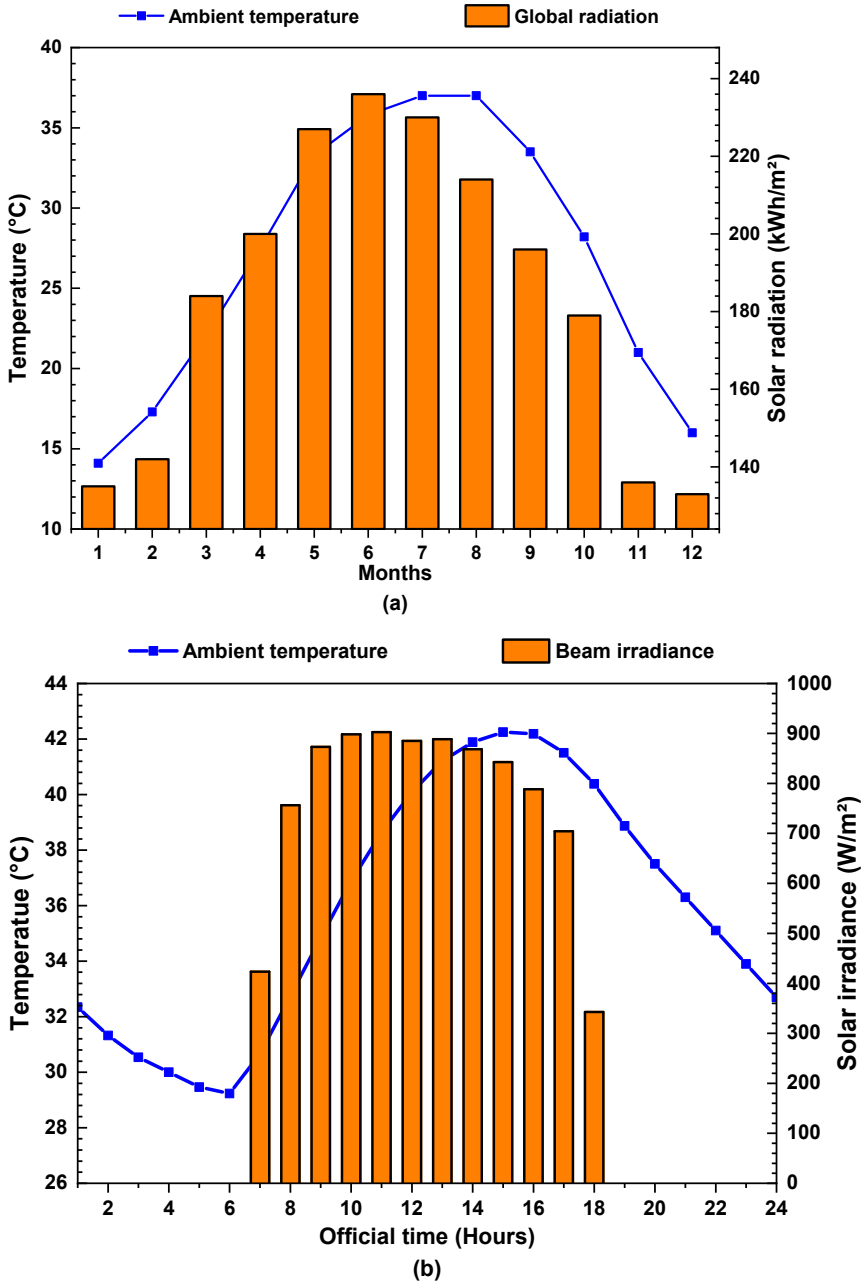

Figure 7. (**a**) Monthly variation and (**b**) hourly variation of ambient temperature and solar radiation in Riyadh (Saudi Arabia).

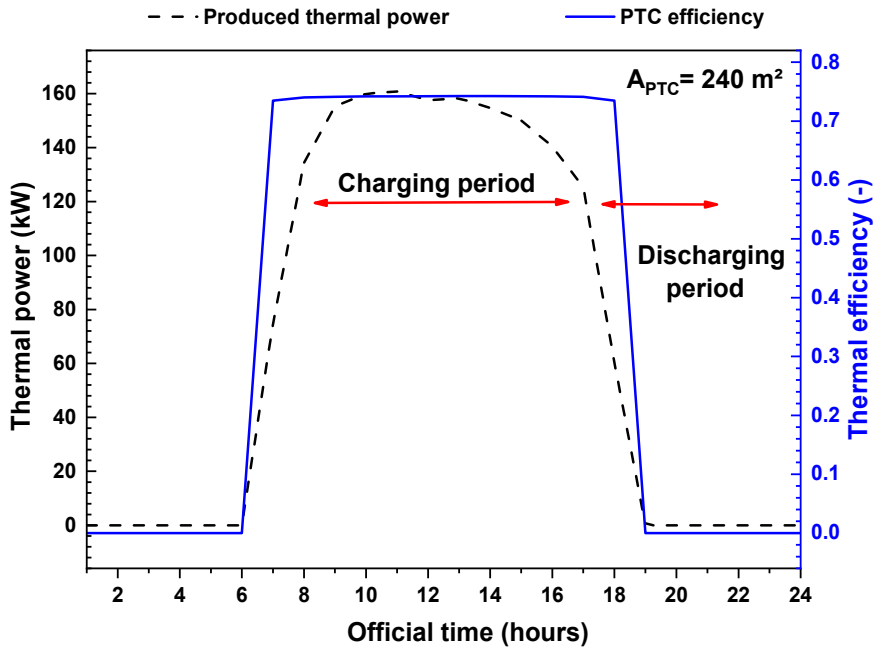

Figure 8. Hourly variation of produced thermal power from the PTC solar field and the PTC thermal efficiency during the 21 June in Riyadh.

4.2.1. PTC Field and PCM Tank Dynamic Behavior

The dynamic behavior of the coupled PTC solar field and PCM tank with the double-effect absorption chiller is presented in this section. Figure 11 illustrates the time-wise evolution of the HTF temperature at the inlet and the outlet of the PTC solar field. This period is assumed from 9:00 a.m. to 5:00 p.m., and the used ambient temperature and received beam radiation are given in Figure 7b. It can be seen that the difference between the HTF inlet and outlet temperatures is about 10.5 °C with a mass flow rate of 13.2 m^3/h; this is a 160-kW solar concentrator thermal power. The HTF temperature at the inlet of the PTC, coming from the PCM tank and the double-effect chiller, increases at the beginning of the system operation before it reaches a stable value of around 118 °C. In fact, the produced hot HTF passes simultaneously through the PCM tank and the chiller generator which leads to a decrease in its temperature. When the PCM melting process starts (at a melting point between 117–119 °C), the HTF inlet temperature stabilizes around this melting point due to the latent heat storage process. After completing the phase process, the HTF temperature at the outlet of the PTC increases and reaches its maximal value of 160 °C. It is interesting to note that the used 160-kW PTC is advantageous for the solar-powered double-effect chiller as the PTC allows the chiller to reach suitable operation temperatures (110–170 °C) during the whole cooling period and also to complete the PCM charging process.

To verify if the PCM tank is completely charged or not (storage process), the variation of PCM temperature at three different locations inside the tank, i.e., top, middle and bottom, is given in Figure 12a. It is interesting to note that the PCM tank is coupled to the solar field and thus the same previous design and operation are used. These results indicate that the PCM temperature at different locations follows the same behavior. At the beginning of the charging operation, the temperature increases until reaching the melting interval (117–119 °C). During this period, only the sensible heat is stored in the tank by increasing the PCM temperature level. When the PCM temperature reaches the melting point, the latent heat storage process starts at a nearly constant temperature. It is interesting to note that the charging process is carried out from the top to the bottom of the PCM tank, which is translated into a rapid increase in the PCM temperature at the top compared to the bottom. Another important parameter during the latent heat storage process is the PCM liquid fraction, which indicates the progress of the physical phase change process (Figure 12b).

As the PCM at the top of the tank is the closest to the hot HTF, its liquid fraction increases quickly compared to other locations, and it reaches a value of 1 (complete charging) after only about 100 min from the beginning of the charging process. However, the PCM located at the bottom of the tank needs about 300 min to become liquid, thus completing the charging process. Overall, the proposed solar-powered system is able to completely charge the PCM tank as all of the PCM becomes liquid during the charging and cooling operation, and therefore both sensible and latent heat is stored in the tank for later use.

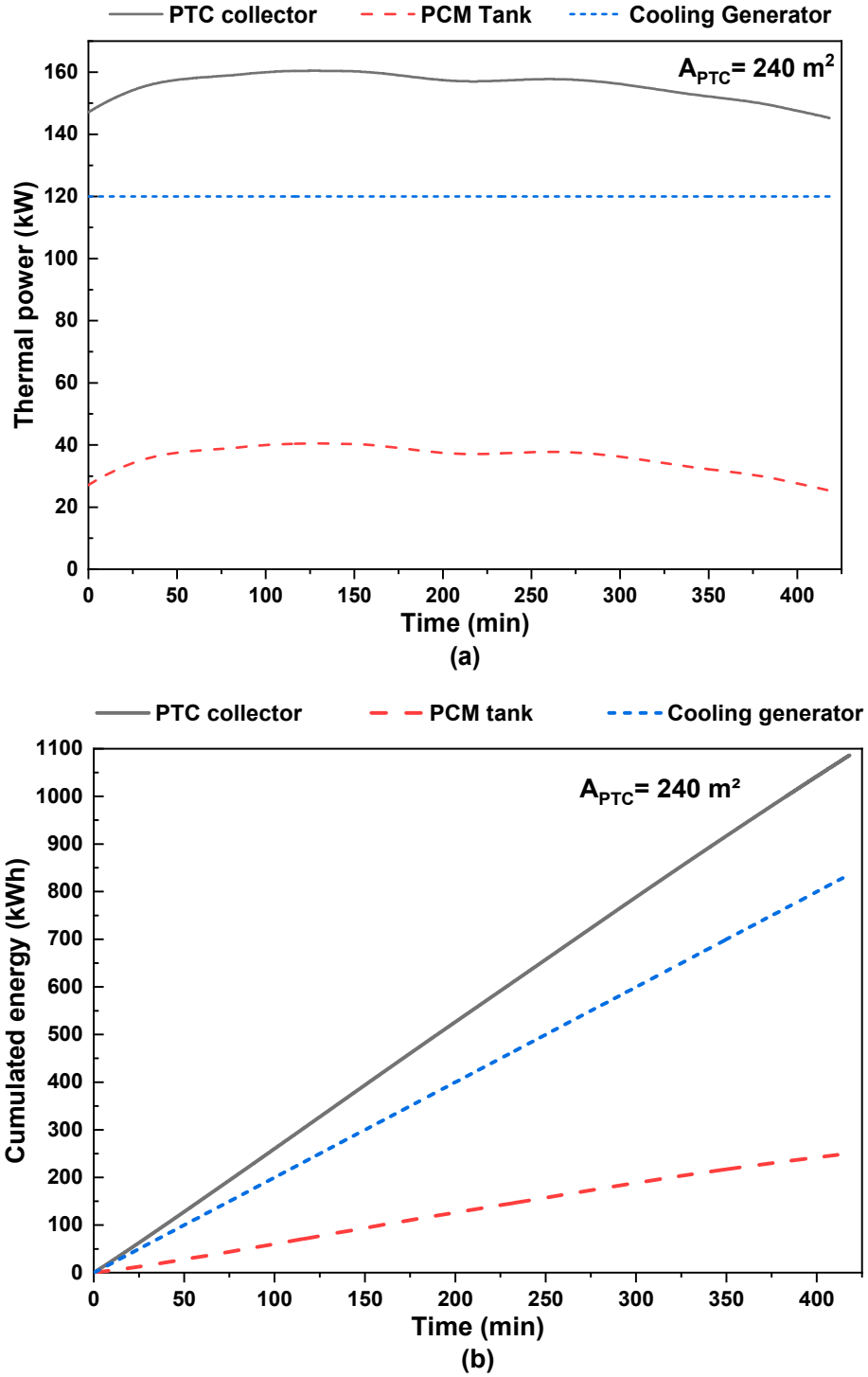

Figure 9. Instantaneous thermal power (**a**) and cumulated thermal energy (**b**): produced by the PTC, stored in the PCM tank and used by the chiller generator for the cooling process.

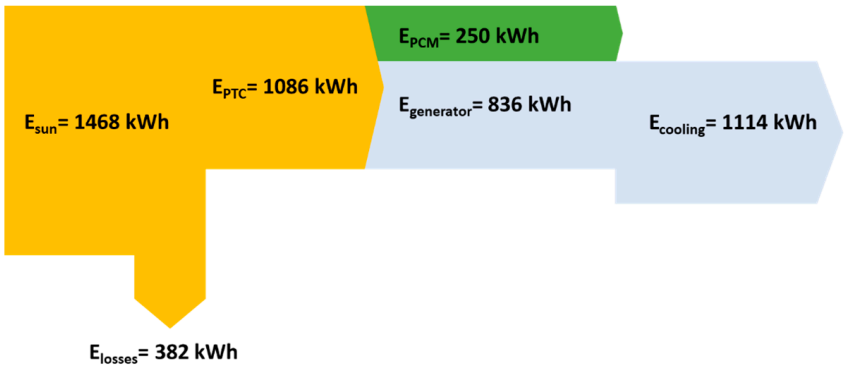

Figure 10. Diagram of energy flow during the charging and cooling process.

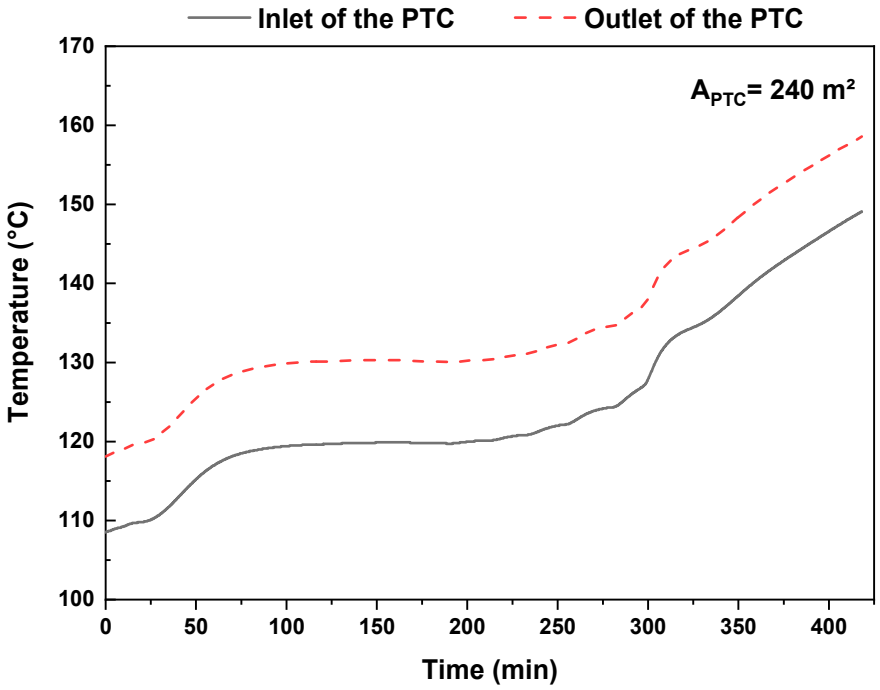

Figure 11. Variation of inlet and outlet HTF temperatures at the PTC solar field.

4.2.2. Effect of the PTC Solar Field Area

To evaluate the influence of the used PTC solar field area on the charging operation, four different PTC areas were used in the developed dynamic model: 200 m^2, 220 m^2, 240 m^2 and 260 m^2. Figure 13a shows the evolution of instantaneously produced solar thermal power from the PTC during the functioning of the coupled PTC–PCM tank-chiller. As expected, increasing the PTC area from 200 m^2 to 260 m^2 leads to an increase in the amount of produced thermal power, and its maximal value varies from 134 kW to 174 kW. The effect of the chosen PTC area on the stored thermal energy is clearly indicated in Figure 13b. It can be seen that reducing the used PTC area leads to a reduction in the amount of stored thermal power in the PCM tank. In fact, the role of the proposed PCM tank is to store only the excess of the produced thermal power. As the necessary thermal power to drive the chiller generator is fixed at 120 kW, minimal stored thermal power is observed for a lower solar PTC field area. The maximal stored thermal power in the PCM tank is equal to 14 kW, 27 kW, 40,5 kW and 54 kW for a PTC area of 200 m^2, 220 m^2, 240 m^2 and 260 m^2, respectively.

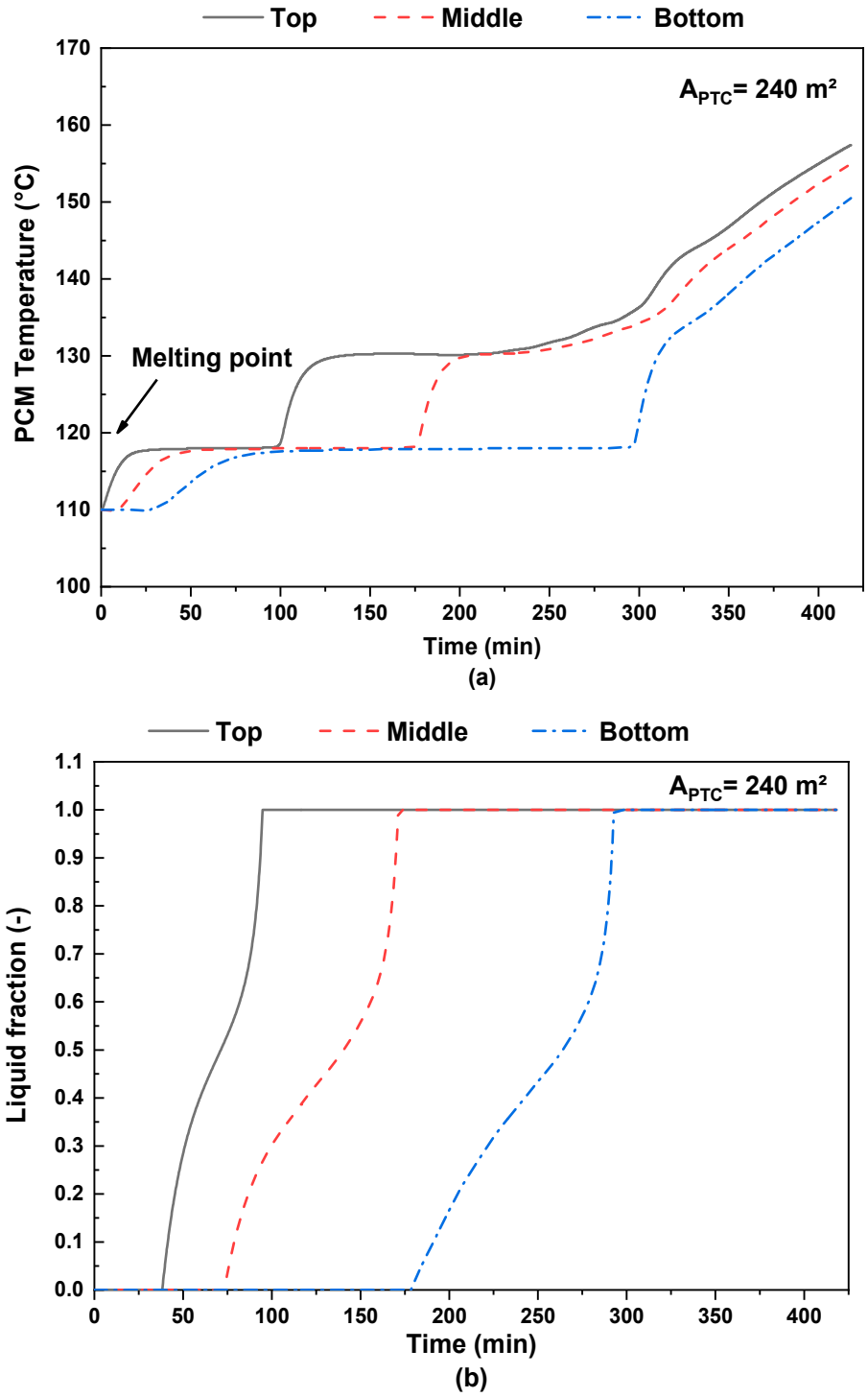

Figure 12. Variation of PCM tank temperature (**a**) and PCM liquid fraction (**b**) during the charging process.

This result could also be presented in the form of a correlation that predicts the produced thermal power from the PTC collector and the stored thermal power in the PCM tank as a function of the PTC area as the following:

$$P_{PTC}(kW) = P_{Base,PTC} + 0.6415(A_{PTC} - A_{PTC,base}) \quad (17)$$

where $P_{Base,PTC}$ is the produced thermal power in kW during the functioning of the system at the base case ($A_{PTC,base} = 200\ m^2$), and A_{PTC} is the actual PTC area.

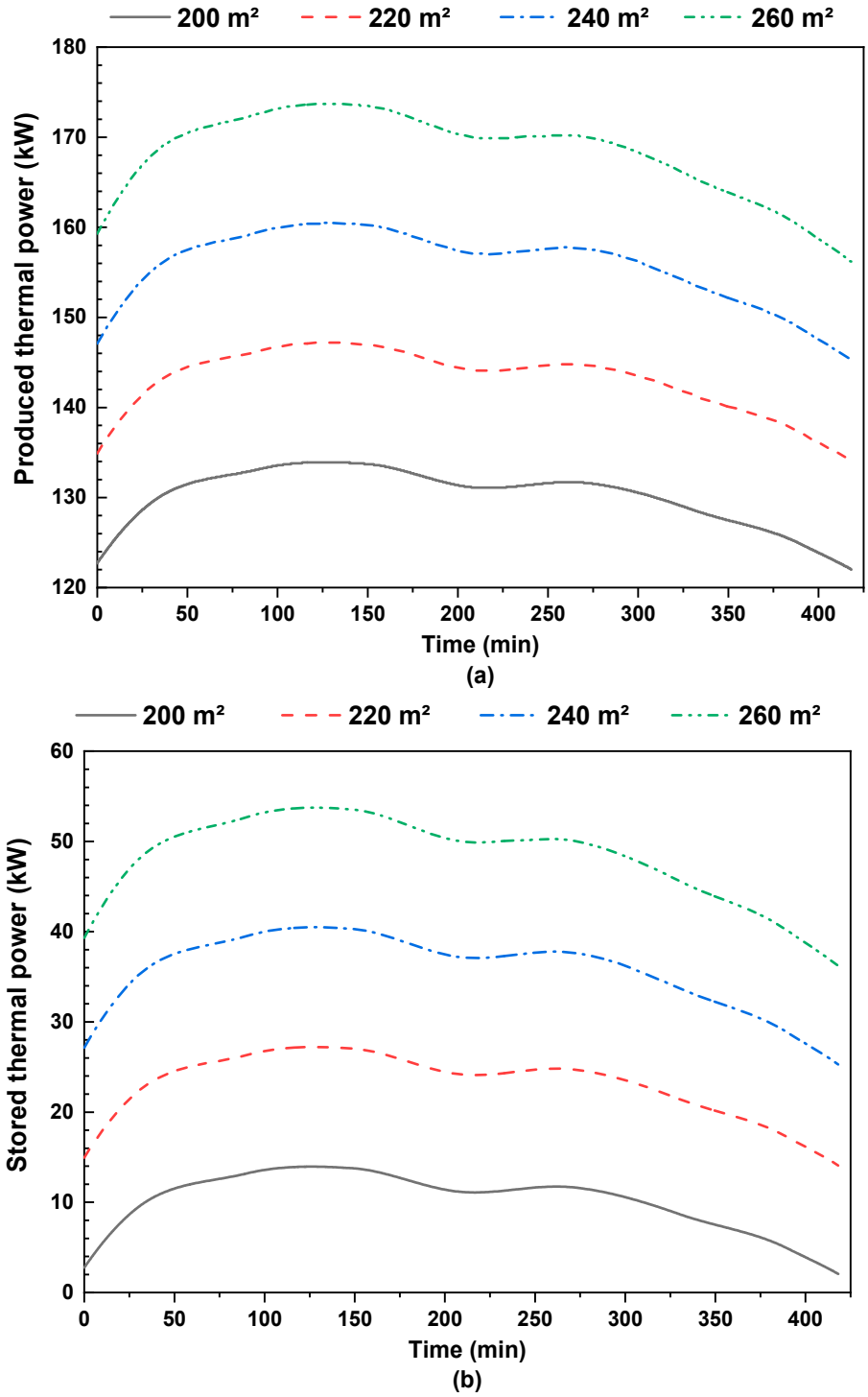

Figure 13. Variation of produced solar thermal power (**a**) and stored thermal power in the PCM tank (**b**).

The same methodology is used to determine the correlation of the stored thermal energy in the PCM storage unit for different values of the PTC area, and it is given as the following:

$$P_{PCM}(kW) = P_{Base} + 0.6093(A_{PTC} - A_{PTC,base}) \quad (18)$$

Figure 14 illustrates the variation of the average PCM liquid fraction during the charging and cooling operation for different values of the PTC solar field. It is worth noting that the cooling need is fixed at 160 kW. These results show that reducing the PTC solar field reduces the PCM storage efficiency by reducing the amount of melted PCM inside

the tank. It can be observed that the phase change kinetic is rapid for the high value of the PTC solar field, and it reaches its suitable value of 1 only for 240 m^2 and 260 m^2 of PTC solar area. The charging time of the PCM tank is reduced by about 45% as the PTC collector area is increased from 220 m^2 to 260 m^2. However, the PCM charging process is not completed for a PTC area lower than 220 m^2. Therefore, it is recommended for the proposed solar-powered system to use a PTC area higher than 220 m^2 in order to ensure a complete charging process of the PCM tank and a stable operation of the 160 kW double-effect absorption chiller.

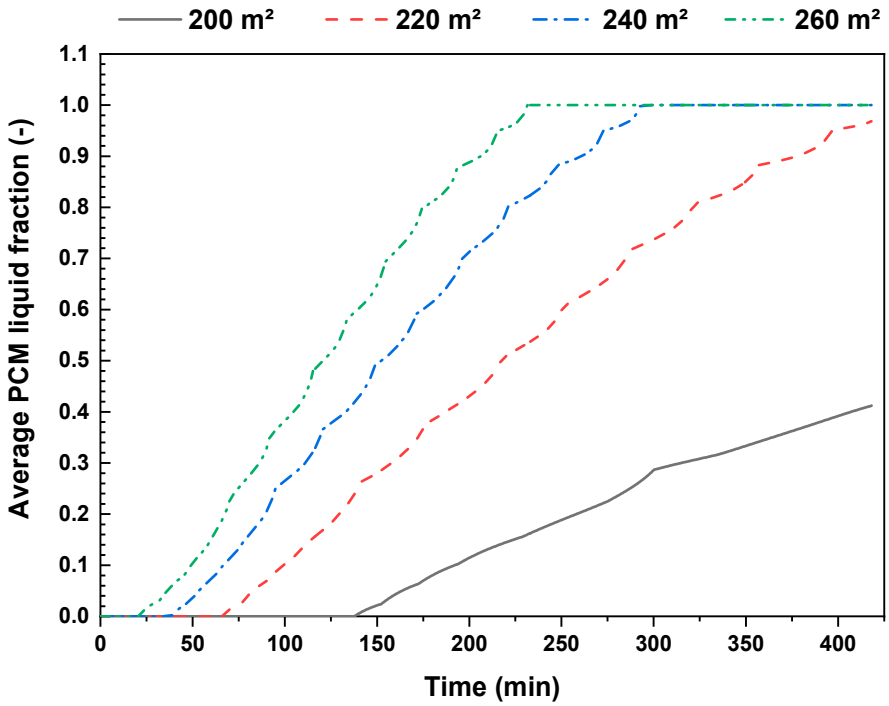

Figure 14. Variation of average PCM liquid fraction during the charging and cooling operation for different PTC field areas.

4.2.3. Effect of the Cooling Power Demand

The influence of the required cooling power needs on the charging operation is investigated in this section. The considered cooling power demands in the double-effect absorption chiller are fixed at 120 kW, 160 kW and 200 kW. It is important to note that during this analysis, the PTC solar field area is fixed at 240 m^2. Figure 15a shows the instantaneous stored thermal power in the PCM tank during the charging operation. This result indicates that the increase in the cooling load demand reduces the amount of stored thermal energy. This behavior is justified by the increase in consumed thermal power by the chiller generator with the cooling load; therefore, the available excess of thermal energy for the PCM storage process is minimal. This cumulated stored thermal power is given in Figure 15b. It can be seen that the maximal amount of stored thermal energy is equal to 450 kWh, 250 kWh and 45 kWh for 120 kW, 160 kW and 200 kW of cooling demand, respectively.

To verify the state of the charging process in the PCM tank, the average PCM liquid fraction at the tank for each cooling power demand is given in Figure 16. It is observed that for all cases, the liquid fraction is equal to zero at the beginning of the charging process which is translated by the sensible heat storage process without change in the PCM physical state. When the PCM temperature reaches the melting interval, the latent heat storage process starts, and the liquid fraction increases. It can be seen that for 120 kW and 160 kW cooling power demand cases, the charging process in the PCM tank is completed, i.e., a liquid fraction equal to 1. The time needed for the charging process is increased by about

64% as the cooling power demand increases from 120 kW to 160 kW. However, for a higher value of cooling power of 200 kW, the use of the present PCM tank is not beneficial as its melting fraction does not exceed 10% and thus its charging process is not completed.

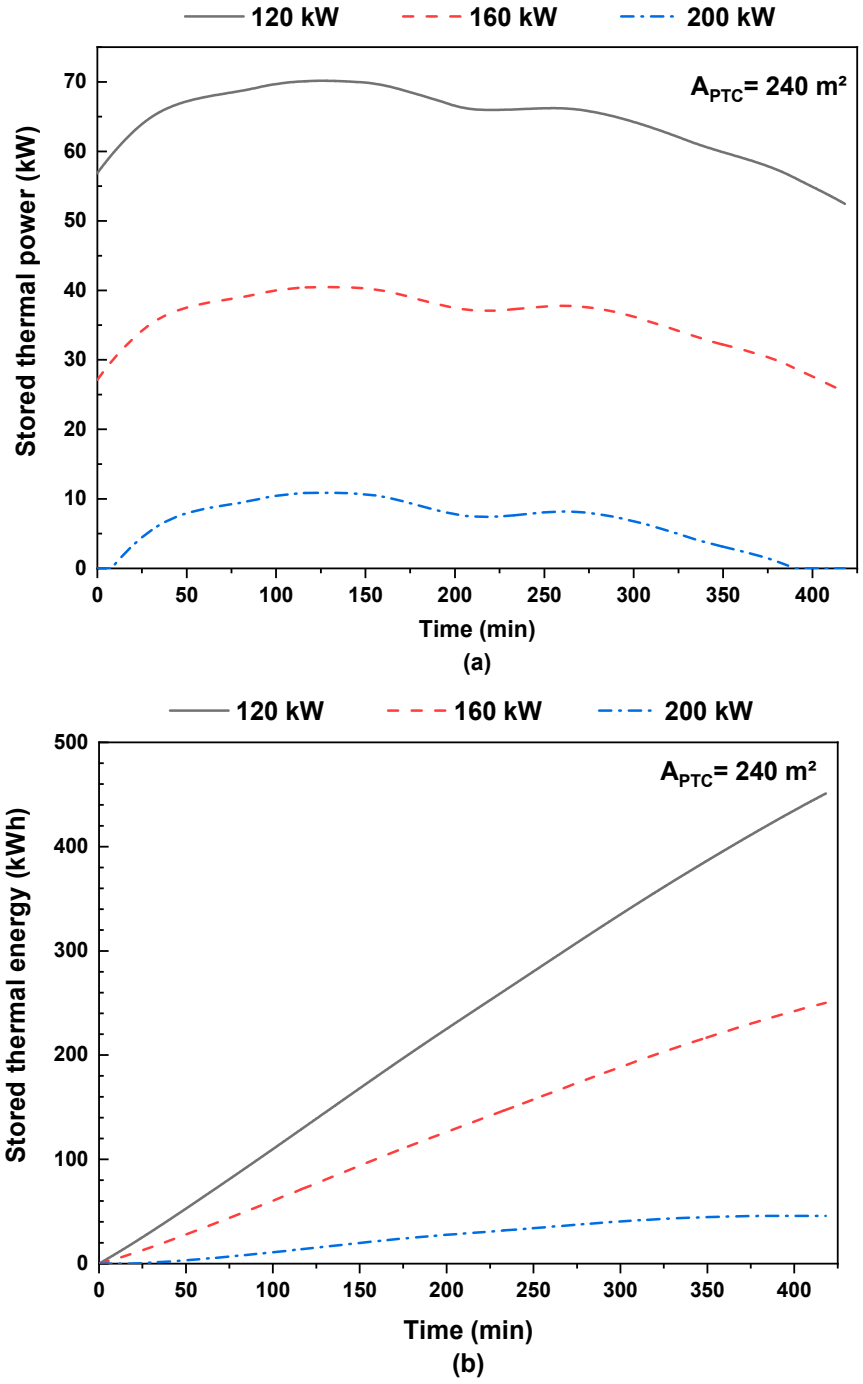

Figure 15. Variation of instantaneous stored thermal power (**a**) and stored thermal energy (**b**) in the PCM tank: influence of the cooling power demand.

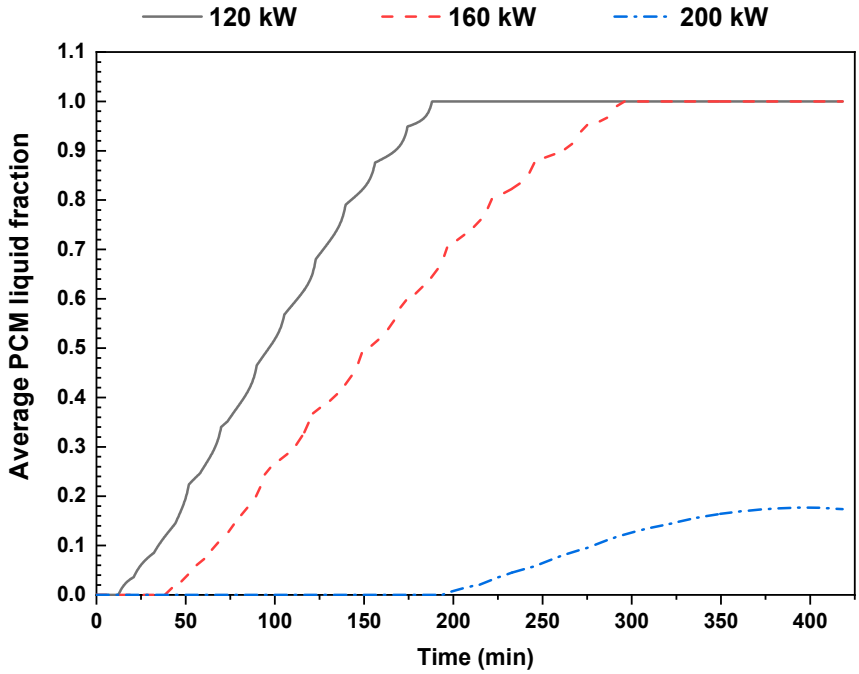

Figure 16. Evolution of PCM average liquid fraction during the charging and cooling operation for different cooling power demands.

4.3. Discharging and Cooling Period

The functioning of the coupled PCM tank and absorption chiller is analyzed in this section, and the potential for using the PCM tank to deliver a part of the necessary thermal energy for driving the chiller generator during the discharging period is investigated. As in the charging period, the cooling power load is fixed at 160 kW and thus the required thermal power to drive the chiller generator is equal to 120 kW (COP = 1.33). This cooling load is assumed to be consumed during the nighttime period for 6 hrs, i.e., from 6:00 p.m. to 11:00 p.m. The main role of the proposed PCM tank is to deliver stored renewable solar thermal power and thus reduce the chiller energy consumption during the nighttime period. The storage system is designed to deliver constant thermal power during the discharging period through the regulation of the HTF mass flow rate. For this purpose, the used pump flow rate is regulated, and it has a minimal mass flow rate of 0.2 kg/s and a maximal one of 1.58 kg/s [33,34]. Initially, the PCM tank is assumed to be charged at a liquid state with an initial temperature of 150 °C (See Section 4.2). If the released thermal power from the PCM is not sufficient to drive the chiller generator, the chiller auxiliary heater will be turned on to deliver additional heat. Figure 17a shows the variation of the HTF temperature at different locations in the PCM tank during the discharging period. It is interesting to note that the discharging process is carried out from the bottom to the top, and the return temperature from the chiller generator is fixed at 110 °C. It can be seen that the HTF temperature increases from the bottom to the top of the tank due to the released thermal energy from the PCM. At the beginning of the discharging period, the HTF outlet temperature (top of the tank) remains constant at 150 °C for about 50 min due to the stored sensible heat in the PCM. After this period, the outlet HTF temperature drops, and it reaches the second plateau where it becomes stable at around 118 °C. This temperature stabilization is advantageous for the chiller operation in stable conditions. During this period, the phase change process of PCM starts and leads to the production of a constant HTF temperature close to the melting interval of the used PCM [117–119 °C] (Figure 17b). At the end of the discharging period, both the outlet HTF temperature and the PCM temperatures at the top of the tank become equal to the inlet temperature (bottom), and the PCM liquid fraction is equal to zero (Figure 17b) (PCM at solid-state).

Figure 17c confirms the advantage of using the proposed PCM tank in the solar-powered cooling system, where it shows its ability to provide the required thermal power of 120 kW. Thanks to the HTF mass flow rate regulation system, the PCM tank provides the necessary thermal power for driving the generator with 120 kW and with a suitable HTF temperature of 150 °C (Figure 17a) during the first hour. As the discharging operation progresses, the delivered thermal power decreases, and the HTF mass flow rate increases and reaches its maximal value of 1.58 kg/s. During this first hour of the discharging period, the backup system of the chiller generator is turned off as the PCM tank is able to deliver all required thermal power for the cooling process (Figure 17c). After this period, the released thermal power from the PCM tank decreases and the chiller auxiliary heater is turned on to provide additional heat.

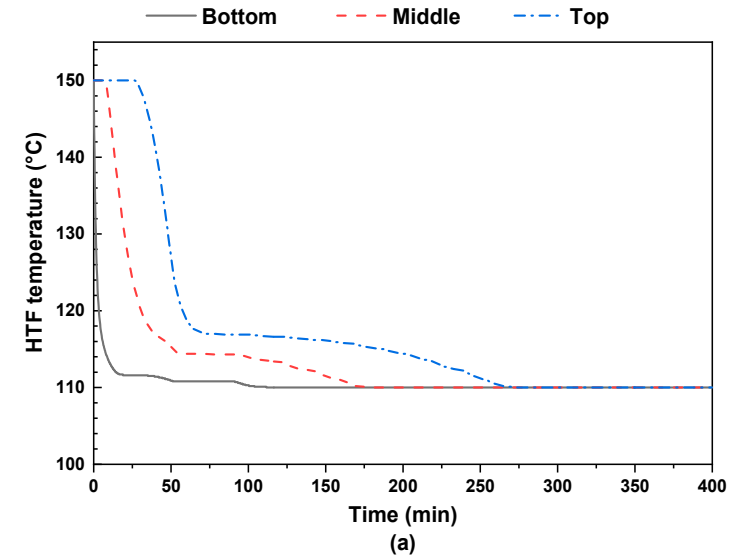

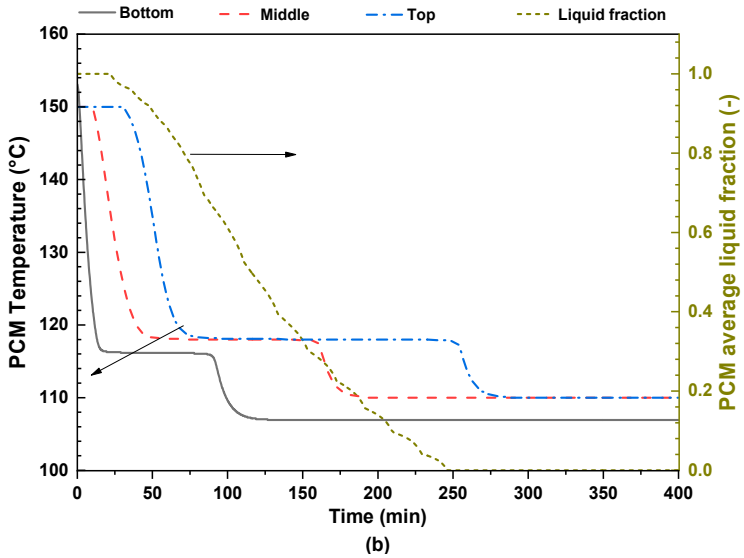

Figure 17. *Cont.*

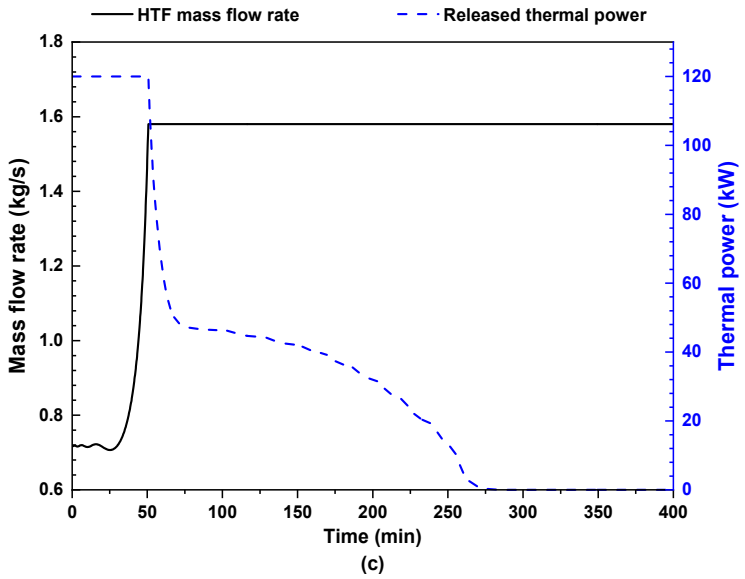

Figure 17. (**a**) Time-wise evolution of the HTF temperature, (**b**) the PCM temperature and liquid fraction in the tank and (**c**) the HTF mass flow rate and the released thermal power.

The advantage of using the PCM tank in the proposed solar-powered cooling system is shown in Figure 18. This figure illustrates the variation of the released thermal energy from the PCM tank and the chiller energy consumption with and without using the PCM tank. The cumulated released thermal energy from the tank increases from the beginning of the discharging process until the end of the operation where it becomes constant and is equal to 240 kWh (end of the discharging). Through analyzing the cooling system with the PCM tank, it can be seen that the chiller energy consumption is equal to zero during the first hour as the PCM tank is able to provide all the necessary thermal power for the cooling process. This result is advantageous compared to the use of sensible storage systems such as water or oil and as proposed by the literature [24,25]. With the progress of the discharging process, the chiller auxiliary heater is turned on as the produced thermal power from the PCM tank is lower than 120 kW (See Figure 17c). Through the comparison of the energy consumption of the two systems (with and without the PCM tank), it can be concluded that using the PCM tank provides a stable operation of the cooling system and reduces its energy consumption by up to 30%.

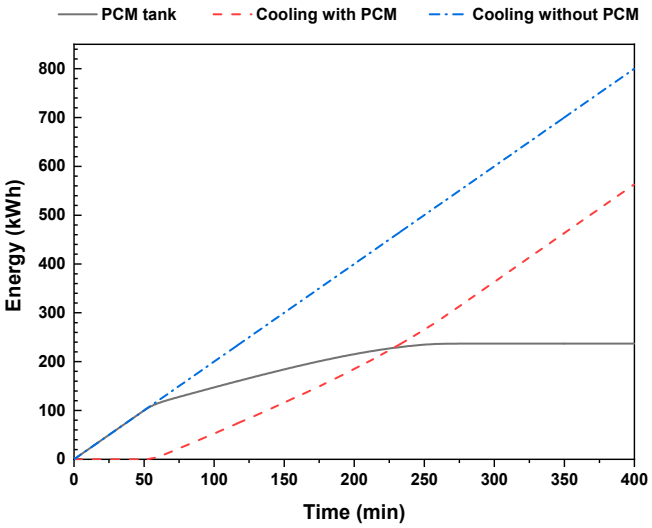

Figure 18. Evolution of released thermal energy from the PCM tank and the chiller energy consumption with and without PCM.

5. Conclusions

A novel solar-powered cooling system coupled with a parabolic trough collector (PTC) and phase change material (PCM) tank is proposed and numerically investigated. The considered water-lithium bromide absorption chiller has a nominal cooling capacity of 160 kW, and it is driven by pressurized hot water under the climatic conditions of Riyadh, Saudi Arabia. A dynamic model for the coupled solar-powered system is developed and validated with experimental measurements from the literature. Both daytime and nighttime operations of the coupled solar cooling system are investigated, and the main results can be concluded as the following:

- Using solar concentrators (PTC) in Riyadh is able to provide necessary thermal power with suitable temperatures ranging from 110 °C to 170 °C for driving double-effect absorption chillers.
- Coupling the PTC collectors with the PCM tank is beneficial for the cooling process due to the PCM tank's ability to store the excess of the produced solar thermal power and to maintain a stable operation of the chiller.
- During the sunny period of the day in Riyadh (from 9 a.m. to 4 p.m.), 77% of produced solar thermal energy from the PTC is used to drive the 160 kW absorption chiller, and 23% is stored in the PCM tank.
- Increasing the PTC area in the solar-powered system from 200 m^2 to 260 m^2 leads to an increase in the amount of produced and stored thermal energy of 22%.
- The charging time of the PCM tank is reduced by about 45% as the PTC collector area is increased from 220 m^2 to 260 m^2.
- By maintaining a fixed PTC area of 240 m^2, the increase in the cooling loads from 120 kW to 200 kW induces a decrease in the stored thermal energy in the PCM tank from 450 kWh to 45 kWh.
- During the nighttime period, the stored thermal energy in the PCM tank is able to continue the cooling process with a stable delivered cooling power of 120 kW and a suitable HTF temperature between 118 °C and 150 °C.
- The use of the PCM tank in the studied absorption chiller leads to a reduction of up to 30% in cooling energy consumption during off-sunshine hours.

Finally, it can be concluded that the proposed solar-powered cooling system with the PTC solar field and the PCM tank is beneficial, and it is recommended for arid regions with high solar radiation and sunny hours. As perspectives of the present work, a detailed environmental analysis and a life cycle cost assessment will be presented and analyzed in future work.

Author Contributions: Conceptualization, E.A. and B.L.; methodology, A.A.; software, B.L.; validation E.A. and B.L.; formal analysis, A.A.; investigation, B.L.; writing—original draft preparation, B.L. and A.A.; writing—review and editing, E.A.; project administration, E.A.; funding acquisition, E.A. All authors have read and agreed to the published version of the manuscript.

Funding: This research was funded by the Agency for Research & Innovation in the Ministry of Education in Saudi Arabia grant number [IFKSUDR_E129] and the APC was funded by the same agency.

Data Availability Statement: The data presented in this study are available in this article.

Acknowledgments: The authors extend their appreciation to the Agency for Research & Innovation in the Ministry of Education in Saudi Arabia for funding this research work through the project number (IFKSUDR_E129).

Conflicts of Interest: The authors declare no conflict of interest.

References

1. El-Sharkawy, I.I.; AbdelMeguid, H.; Saha, B.B. Potential Application of Solar Powered Adsorption Cooling Systems in the Middle East. *Appl. Energy* **2014**, *126*, 235–245. [CrossRef]
2. Li, Q.; Zhao, S.; Wang, D.; Song, Q.; Zhou, S.; Wang, X.; Li, Y. Simulation Study on Solar Single/Double-Effect Switching LiBr-H_2O Absorption Refrigeration System. *Energies* **2023**, *16*, 3220. [CrossRef]

3. Al-Yasiri, Q.; Szabó, M.; Arıcı, M. A Review on Solar-Powered Cooling and Air-Conditioning Systems for Building Applications. *Energy Rep.* **2022**, *8*, 2888–2907. [CrossRef]
4. IAE. IAE District-Heating. Available online: https://www.iea.org/reports/district-heating (accessed on 1 March 2023).
5. Alahmer, A.; Ajib, S. Solar Cooling Technologies: State of Art and Perspectives. *Energy Convers. Manag.* **2020**, *214*, 112896. [CrossRef]
6. Aljuhani, Y.; Dayem, A.M.A. Thermal Analysis of a Solar-Powered Absorption Air-Conditioning System: Case Study for a Tent in Mina Zone, Saudi Arabia. *Clean. Eng. Technol.* **2022**, *8*, 100472. [CrossRef]
7. Al-Ugla, A.A.; El-Shaarawi, M.A.I.; Said, S.A.M. Alternative Designs for a 24-Hours Operating Solar-Powered LiBr–water Absorption Air-Conditioning Technology. *Int. J. Refrig.* **2015**, *53*, 90–100. [CrossRef]
8. Rahman, A.; Abas, N.; Dilshad, S.; Saleem, M.S. A Case Study of Thermal Analysis of a Solar Assisted Absorption Air-Conditioning System Using R-410A for Domestic Applications. *Case Stud. Therm. Eng.* **2021**, *26*, 101008. [CrossRef]
9. Habib, M.F.; Ali, M.; Sheikh, N.A.; Badar, A.W.; Mehmood, S. Building Thermal Load Management through Integration of Solar Assisted Absorption and Desiccant Air Conditioning Systems: A Model-Based Simulation-Optimization Approach. *J. Build. Eng.* **2020**, *30*, 101279. [CrossRef]
10. Rahman, S.; Said, Z.; Issa, S. Performance Evaluation and Life Cycle Analysis of New Solar Thermal Absorption Air Conditioning System. *Energy Rep.* **2020**, *6*, 673–679. [CrossRef]
11. Narayanan, R.; Harilal, G.K.; Golder, S. Feasibility Study on the Solar Absorption Cooling System for a Residential Complex in the Australian Subtropical Region. *Case Stud. Therm. Eng.* **2021**, *27*, 101202. [CrossRef]
12. Lahoud, C.; El Brouche, M.; Lahoud, C.; Hmadi, M. A Review of Single-Effect Solar Absorption Chillers and Its Perspective on Lebanese Case. *Energy Rep.* **2021**, *7*, 12–22. [CrossRef]
13. Khan, M.I.; Asfand, F.; Al-Ghamdi, S.G. Progress in Research and Technological Advancements of Thermal Energy Storage Systems for Concentrated Solar Power. *J. Energy Storage* **2022**, *55*, 105860. [CrossRef]
14. Ali, M.; Alkaabi, A.K.; Lee, J.I. CFD Simulation of an Integrated PCM-Based Thermal Energy Storage within a Nuclear Power Plant Connected to a Grid with Constant or Variable Power Demand. *Nucl. Eng. Des.* **2022**, *394*, 111819. [CrossRef]
15. Ali, M.; Alkaabi, A.K.; Addad, Y. Numerical Investigation of a Vertical Triplex-Tube Latent Heat Storage/exchanger to Achieve Flexible Operation of Nuclear Power Plants. *Int. J. Energy Res.* **2022**, *46*, 2970–2987. [CrossRef]
16. Yadav, V.K.; Sarkar, J.; Ghosh, P. Thermodynamic, Economic and Environmental Assessments of a Novel Solar-Driven Combined Cooling and Power System. *J. Clean. Prod.* **2023**, *402*, 136791. [CrossRef]
17. Ghaith, F.A.; Onur Dag, R. Performance and Feasibility of Utilizing Solar Powered Ice Storage System for Space Cooling Applications. *Energy Convers. Manag. X* **2022**, *16*, 100319. [CrossRef]
18. Ibrahim, N.I.; Al-Sulaiman, F.A.; Saat, A.; Rehman, S.; Ani, F.N. Charging and Discharging Characteristics of Absorption Energy Storage Integrated with a Solar Driven Double-Effect Absorption Chiller for Air Conditioning Applications. *J. Energy Storage* **2020**, *29*, 101374. [CrossRef]
19. BROAD USA. Available online: https://broadusa.com/broad/absorption-chiller/ (accessed on 3 March 2023).
20. Lamrani, B.; Khouya, A.; Zeghmati, B.; Draoui, A. Mathematical Modeling and Numerical Simulation of a Parabolic Trough Collector: A Case Study in Thermal Engineering. *Therm. Sci. Eng. Prog.* **2018**, *8*, 47–54. [CrossRef]
21. Lamrani, B.; Kuznik, F.; Draoui, A. Thermal Performance of a Coupled Solar Parabolic Trough Collector Latent Heat Storage Unit for Solar Water Heating in Large Buildings. *Renew. Energy* **2020**, *162*, 411–426. [CrossRef]
22. Kalogirou, S.A. Parabolic Trough Collectors for Industrial Process Heat in Cyprus. *Energy* **2002**, *27*, 813–830. [CrossRef]
23. Kalogirou, S.A. Solar Thermal Collectors and Applications. *Prog. Energy Combust. Sci.* **2004**, *30*, 231–295. [CrossRef]
24. Tzivanidis, C.; Bellos, E.; Antonopoulos, K.A. Energetic and Financial Investigation of a Stand-Alone Solar-Thermal Organic Rankine Cycle Power Plant. *Energy Convers. Manag.* **2016**, *126*, 421–433. [CrossRef]
25. Bellos, E.; Tzivanidis, C.; Pavlovic, S.; Stefanovic, V. Thermodynamic Investigation of LiCl-H_2O Working Pair in a Double Effect Absorption Chiller Driven by Parabolic Trough Collectors. *Therm. Sci. Eng. Prog.* **2017**, *3*, 75–87. [CrossRef]
26. Dudley, V.; Kolb, G.; Mahoney, A.; Mancini, T.; Mattews, C.; Sloan, M. *Test Results: SEGS LS-2 Solar Collector*; Report of Sandia National Laboratories (SAND94-1884); Sandia National Laboratories: Albuquerque, NM, USA, 1994.
27. Bellos, E.; Tzivanidis, C. A Detailed Exergetic Analysis of Parabolic Trough Collectors. *Energy Convers. Manag.* **2017**, *149*, 275–292. [CrossRef]
28. Lamrani, B.; Draoui, A. Modelling and Simulation of a Hybrid Solar-Electrical Dryer of Wood Integrated with Latent Heat Thermal Energy Storage System. *Therm. Sci. Eng. Prog.* **2020**, *18*, 100545. [CrossRef]
29. Lamrani, B.; Johannes, K.; Kuznik, F. Phase Change Materials Integrated into Building Walls: An Updated Review. *Renew. Sustain. Energy Rev.* **2021**, *140*, 110751. [CrossRef]
30. PlusICE®. Available online: https://www.pcmproducts.net/ (accessed on 3 March 2023).
31. Lamrani, B.; Eddine, B.; Khattari, Y.; Kousksou, T. A Simplified Thermal Model for a Lithium-Ion Battery Pack with Phase Change Material Thermal Management System. *J. Energy Storage* **2021**, *44*, 103377. [CrossRef]
32. Lebrouhi, B.E.; Lamrani, B.; Ouassaid, M.; Abd-Lefdil, M.; Maaroufi, M.; Kousksou, T. Low-Cost Numerical Lumped Modelling of Lithium-Ion Battery Pack with Phase Change Material and Liquid Cooling Thermal Management System. *J. Energy Storage* **2022**, *54*, 105293. [CrossRef]

33. Lamrani, B.; Belcaid, A.; Lebrouhi, B.E.; El Rhafiki, T.; Kousksou, T. Numerical Investigation of a Latent Cold Storage System Using Shell-and-Tube Unit. *Energy Storage Sav.* **2023**, 1–32. [CrossRef]
34. Lamrani, B.; Belcaid, A.; Lebrouhi, B.E.; Khodadadi, J.M.; El Rhafiki, T. Dynamic Thermal Analysis of a Coupled Solar Water Heaters-Thermal Storage Tank for Solar Powered District Heating Networks. *J. Energy Storage* **2023**, *61*, 106793. [CrossRef]
35. Medved, I.; Trník, A.; Vozár, L. Modeling of Heat Capacity Peaks and Enthalpy Jumps of Phase-Change Materials Used for Thermal Energy Storage. *Int. J. Heat Mass Transf.* **2017**, *107*, 123–132. [CrossRef]
36. Halimov, A.; Lauster, M.; Müller, D. Validation and Integration of a Latent Heat Storage Model into Building Envelopes of a High-Order Building Model for Modelica Library AixLib. *Energy Build.* **2019**, *202*, 109336. [CrossRef]
37. Klein, S.A.; Alvarado, F. *EES: Engineering Equation Solver*; F-Chart Software: Madison, WI, USA, 1999.
38. Bentivoglio, F.; Rouge, S.; Soriano, O.; Tempass de Sousa, A. Design and Operation of a 180 kWh PCM Heat Storage at the Flaubert Substation of the Grenoble Urban Heating Network. *Appl. Therm. Eng.* **2021**, *185*, 116402. [CrossRef]
39. Lamrani, B.; Kousksou, T. Numerical Investigation of a Shell-and-Tube Latent Heat Thermal Energy Storage System for Urban Heating Network. *J. Energy Storage* **2021**, *43*, 103216. [CrossRef]